
Article:
Westmoreland, S. C., Evans, R. F.L. orcid.org/0000-0002-2378-8203, Hrkac, G. et al. (10 more authors) (2018) Multiscale model approaches to the design of advanced permanent magnets. Scripta Materialia. pp. 56-62. ISSN 1359-6462

https://doi.org/10.1016/j.scriptamat.2018.01.019

Multiscale model approaches to the design of advanced permanent magnets

S.C. Westmoreland[a,*], R.F.L. Evans[a], G. Hrkac[b], T. Schrefl[c], G.T. Zimanyi[d], M. Winklhofer[e], N. Sakuma[f], M. Yano[f], A. Kato[f], T. Shoji[f], A. Manabe[f], M. Ito[f], R.W. Chantrell[a]

[a] *Department of Physics, University of York, Heslington, York YO10 5DD, United Kingdom*
[b] *CEMPS, Harrison Building, University of Exeter, Exeter EX4 4QF, United Kingdom*
[c] *Center for Integrated Sensor Systems, Danube University Krems, Austria*
[d] *Department of Physics, University of California, Davis, California 95616, USA*
[e] *Carl von Ossietzky University of Oldenburg, 26129 Oldenburg, Germany*
[f] *Toyota Motor Corporation, 1200 Mishuku, Susono, Shizuoka 410-1193, Japan*

Abstract

We describe the process of multiscale modelling of magnetic materials, based on atomistic models coupled parametrically to micromagnetic calculations. At the atomistic lengthscale we use Spin Dynamics (SD) to study switching mechanisms, using structures predicted by Molecular Dynamics. The process is completed using SD to calculate the cell size and temperature dependent parameters for micromagnetic calculations. We demonstrate an unusually strong cell size scaling for $Nd_2Fe_{14}B$, and demonstrate numerically the existence of atomic scale Barkhausen jumps during magnetization switching. Scaling of magnetic properties is shown to be important in micromagnetic calculations of hysteresis, especially considering variation in micromagnetic cell size.

1. Introduction

Micromagnetics is the computational tool of choice for permanent magnet modelling. However, following the proposal of exchange spring magnets by Kneller and Hawig [1] to optimise magnetic properties by coupling a (soft) high moment material with a (hard) low moment material, permanent magnets have been increasingly designed at the nanoscale to achieve the desired functionality. The high remanent magnetization arises due to the high Fe content in the alloy, while the origin of the coercivity combines intrinsic properties of the hard phase (the anisotropy) and extrinsic properties which are intimately tied to the material microstructure [2, 3, 4, 5]. Understanding the links between material properties, microstructure and magnetic properties is vital for the optimisation of magnetic properties including the energy product.

Micromagnetic models can be used to investigate the magnetic behaviour of such systems, and remain vital for large scale calculations: for example micromagnetic modelling shows the potential advantages of complex designs such as the 'Battenburg' structure [6]. However, they do not have access to the effect of the detailed interface structure at the atomic level and its effect on intrinsic magnetic properties, which might be expected to have a bearing on the model predictions. A further difficulty is the scaling of magnetic properties with cell size. This was first investigated by Dobrovitski et. al. [7] and Grinstein and Koch [8]. The coarse-grained micromagnetic variables tend to lead to an over-estimate of T_c which is shown to be removed by a renormalisation approach [8]. Essentially this means the that the anisotropy and saturation magnetization and also the exchange stiffness constant must be taken as cell-size (L) and temperature dependent, i.e., $K = K(T, L)$, $M_s = M_s(T, L)$ and $A = A(T, L)$. Here we show that these variations can be calculated using atomistic model simulations, linking atomistic and micromagnetic models in a multiscale approach. This is especially important for automotive and other applications involving high temperature operation.

In a world with infinite compute resources one could imagine quantum-based materials simulations, however this is unlikely to be achievable in the foreseeable future. The only feasible approach is to couple and link the formalisms associated with each lengthscale (an overview of this process is shown in Fig. 1). These are

1. *Ab-initio calculations.* These involve the solution of the quantum mechanical problem of interacting electrons. The most common formalism: Density Functional Theory (DFT), essentially transforms the many-body Schrödinger equation into a problem of determining local electron densities. DFT is highly successful in predicting materials properties, at least to the extent of interatomic potentials: a fact central to the Molecular Dynamics modelling to be described in section 2. However, the energies associated with important magnetic properties, especially anisotropy energies are very small. In addition, the determination of anisotropy values by DFT requires relativistic corrections and is a rather difficult and specialised

*Corresponding author
Email address: sw766@york.ac.uk (S.C. Westmoreland)

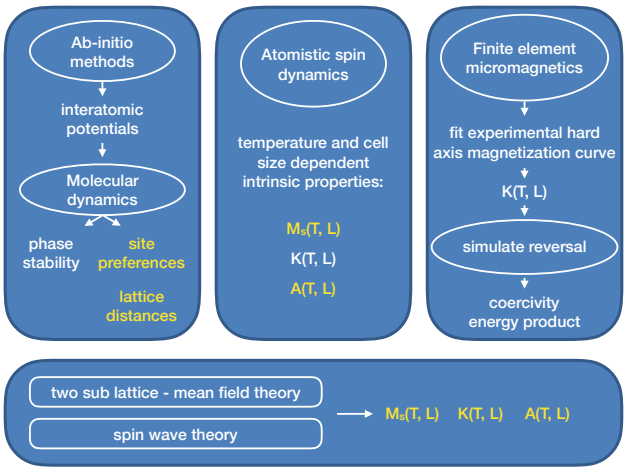

Figure 1: Schematic of the multiscaling process for magnetic materials. The arrows indicate the interactions between the various computational and analytical approaches and show the paths taken for the exchange of information between the model lengthscales. While the mean field and spin wave theories are beyond the scope of this review they are included for completeness, showing their important role in verification of numerical approaches.

area. Further limitations of DFT are that firstly it is strictly valid at zero Kelvin and secondly CPU requirements limit the calculations to a few hundred atoms.

2. *Atomistic Spin Dynamics (SD) calculations.* SD models make the (adiabatic) approximation of a classical atomic spin of fixed length able to rotate freely. The exchange interaction between spins is generally taken as being of Heisenberg form. In principle, the first stage of the multiscaling process is to determine the important parameters (spin values, exchange and anisotropy) from the ab-initio calculations. Importantly, the atomistic approach allows a thermodynamic treatment of the spin system leading to predictions of the temperature variation of magnetic properties and also of dynamic behaviour at elevated temperatures. In addition to providing a powerful and predictive approach in its own right, the atomistic approach provides the basic input to micromagnetic models in the form of temperature and cell size dependent properties. Atomistic models are currently limited to systems if 10^6 to 10^8 spins and timscales of up to ~ 100 nanoseconds.
3. *Micromagnetic calculations.* These extend the lengthscale and timescale of calculations by orders of magnitude, but lose direct connection to the underlying physics expressed by the *ab-initio* models. The final link in the multiscale chain is to introduce atomistically calculated values of temperature and cell-size dependent properties into the model.
4. *Molecular Dynamics (MD).* While 1-3 represent the magnetic aspects of the multiscale chain, the use of interfaces to provide the functionality of modern magnetic materials requires special consideration. For example, the hard/soft interfaces in exchange spring magnets are likely to influence the magnetic properties in a complicated way due to, for example, stresses arising from lattice mismatch. This is the province of MD, which uses classical equations of motion driven by *ab-initio* parameterised force fields to predict structures of materials and interfaces. Here we use MD calculations of the $Nd_2Fe_{14}B/\alpha-Fe$ interfaces to predict interface anisotropy values and use them in atomistic calculations of domain wall propagation across the interface.

The multiscale approach to magnetic materials simulations was first proposed for FePt due to its importance as the material of choice for ultra-high density magnetic storage based on heat assisted magnetic recording (HAMR) [9]. The basic approach, described by Kazantseva et. al., [10] is firstly to use *ab-initio* methods to determine the main magnetic parameters [11]. These are used to determine the main parameters for the atomistic spin model. Subsequently, the atomistic model is used to determine the temperature dependent parameters for macrospin models of magnetic recording. Although pictured here as an intermediate model linking *ab-initio* and macroscopic models, atomistic approaches are important in their own right in essentially merging the quantum (*ab-initio*) and thermodynamic regimes, leading to, for example important insights into HAMR and also the prediction of thermally assisted magnetization switching [12, 13]. The multiscale approach is in an early stage of development for permanent magnets. As will be discussed later, this is at least partially due to the difficulty of obtaining reliable *ab-initio* information on the magnetic properties of rare-earths, which necessitates the determination of magnetic parameters by fitting to experiment. Here we outline the overall approach, describing first the molecular dynamic model of interface structures. We then outline the SD model development and the techniques for determination of the important intrinsic atomic parameters, including the calculation of the anisotropy arising from symmetry breaking due to stresses in the soft phase at an interface between $Nd_2Fe_{14}B$ and $\alpha-Fe$.

2. Molecular dynamics model of interface properties

To be able to understand solids and calculate material parameters such as magnetocrystalline anisotropy it is necessary to use molecular dynamics and first principle studies, for the first, in particular molecular force fields to extract physical and chemical properties at bulk and thin film level.

This was shown in our previous work [14, 15] where we investigated metallic Nd grain boundary phases and fcc and hcp Nd-rich phases by using Morse potentials. Recent investigations have shown, if there are different Nd-O grain

boundary phases depending on the oxygen content in the production process a mixed MD approach has to be used.

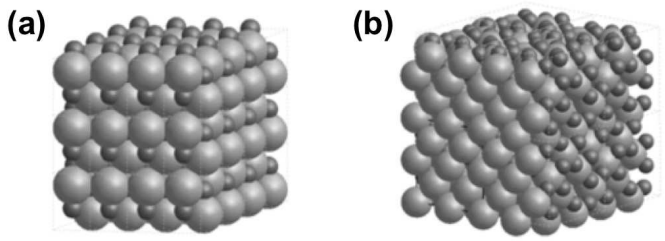

Figure 2: (a) Calculated unit cell of Nd_2O_3-hP5 using Buckingham potentials in a constant pressure calculation, lattice parameters a = 3.8221 and c = 6.105 . (b) Calculated unit cell of a Nd_2O_3-cI80 using Buckingham potentials in a constant pressure calculation, lattice parameter $a = 11.0564$, in excellent agreement with the experimental values.

The atomistic structures of the systems involved are simulated using energy minimization codes such as the GULP code [16]. As the systems can be comprised of both metallic (e.g. $Nd_2Fe_{14}B$, fcc-Nd, dhcp-Nd) and oxide (e.g. Nd_2O_3-hP5, Nd_2O_3-cI80 and NdO) phases, one has to employ different empirical potential models for the interatomic interactions for each system. In the metallic systems it is possible to ignore the Coulombic forces in the system as each atom is formally charge neutral. However, in the oxide phases the atomic centres carry a formal charge, as a result there is a transfer of electrons from the metal atom to the oxygen, due to their different electronegativities. Therefore a Coulomb term must be calculated from these interactions. A good candidate to simulate oxide interactions is the Buckingham potential. This potential, that describes the Pauli repulsion energy and the van der Waals energy, has the form

$$\Phi_{sr}(r_{ij}) = A_{ij} \exp\left(\frac{r_{ij}}{\rho_{ij}}\right) - \frac{C_{ij}}{r_{ij}^6} \qquad (1)$$

where A_{ij} and ρ_{ij} describe the repulsion interaction, related to the electron number and electron density, while C_{ij} describes the attractive energy. The results of such a simulation are shown in Fig. 2. The parameters in our model were adapted from a La-O potential and fitted to the inter-atomic separation of Nd-O. This model, which incorporates a core-shell separation of the charge [17] on oxygen that accounts for the polarizability of the oxygen atoms, is validated against experimental data for Nd_2O_3 crystal structures.

The metallic phase is modeled with a Morse potential with the form

$$\Phi_{sr}(r_{ij}) = D_{ij}[1 - \exp(-\beta_{ij}\{r_{ij} - r_0\})]^2 \qquad (2)$$

where D_{ij} is the disassociation energy of the bond and β_{ij} is a variable parameter that can be determined from spectroscopic data. This type of model is particularly useful in chemical systems to model bonded covalent interactions. The parameters for these interactions are taken from the work of Chen *et al.* [18].

The interfaces of mixed systems are constructed with crystallographic orientations as determined by TEM or SEM. Due to the different lattice parameters on either side of the interface it is necessary to use super cells of each phase to reduce the interface surface matching error, which would result in an incoherent interface system.

The potential energy of the system was minimised via the Newton Raphson method in GULP [16]. The strain on the atoms was calculated from the displacement of each atom from its original position in the super cell structure. From the strain the change in magnetoelastic anisotropy was calculated as follows [19, 20, 21, 22]. A linear strain was assumed (harmonic approximation), which corresponds to a one-ionic magnetoelastic coupling. The bulk strain description in the Voigt notation is used [19], leaving a 3 by 3 tensor system with six unknowns. To reduce the complexity, orthorhombic distortions were neglected and tetragonal symmetry was assumed [20, 23].

First, the symmetrised strain in the tetragonal system was calculated from the Cartesian strain components obtained from lattice minimisation calculations. This allows an approach, via the magnetoelastic coefficients, to obtain the first-order magnetoelastic anisotropy constant K_{me} [22], the magnetoelastic energy [21], and the penetration depth of the distortions.

3. Basis of the atomistic spin model approach

The SD approach is constructed on an intermediate lengthscale between *ab-initio* and micromagnetic calculations. As such it is both a central link in the multiscale chain and also, as mentioned previously, an important physical model approach in its own right. It is based on the approximation of a fixed length atomic spin and the Heisenberg approach to magnetic exchange. Although in principle this is a limited approach, we note that more complex materials such as FeRh can be treated with higher order four-spin exchange terms [24, 25], which may be thought of as a representation of complex hopping processes associated with indirect exchange.

3.1. The classical spin Hamiltonian

The Heisenberg spin model encapsulates the essential physics of a magnetic material at the atomic level. The spin Hamiltonian $\mathcal{H}$ typically has the form:

$$\mathcal{H} = \mathcal{H}_{\text{exc}} + \mathcal{H}_{\text{ani}} + \mathcal{H}_{\text{app}} \qquad (3)$$

denoting terms for the exchange interaction, magnetic anisotropy, and externally applied magnetic fields respectively.

The dominant term in the spin Hamiltonian is the exchange energy. Rather than using the micromagnetic approximation (valid for long wavelengths), the exchange energy for a system of interacting atomic moments is taken

as the Heisenberg form:

$$\mathcal{H}_{\rm exc} = -\sum_{i<j} J_{ij}\mathbf{S}_i \cdot \mathbf{S}_j \tag{4}$$

where J_{ij} is the exchange interaction between atomic sites i and j, $\mathbf{S}_i$ is a unit vector denoting the local spin moment direction and $\mathbf{S}_j$ is the spin moment direction of neighboring atoms. Due to the strong distance dependence of the exchange interaction the sum in Eq. 4 is often truncated to include nearest neighbours only. This significantly reduces the computational effort while being a good approximation for many materials of interest. In reality, however, the exchange interaction can extend to several atomic spacings [26, 27], representing hundreds of pairwise interactions.

In the simplest case the exchange interaction J_{ij} is isotropic, meaning that the exchange energy of two spins depends only on their relative orientation. In more complex materials, the exchange interaction forms a tensor with components:

$$\mathbf{J}_{ij}^{T} = \begin{bmatrix} J_{xx} & J_{xy} & J_{xz} \\ J_{yx} & J_{yy} & J_{yz} \\ J_{zx} & J_{zy} & J_{zz} \end{bmatrix}, \tag{5}$$

which is capable of describing *anisotropic* exchange interactions, such as two-ion anisotropy [26] and the Dzyaloshinskii-Moriya interaction (off-diagonal components of the exchange tensor). In the case of tensorial exchange, the exchange energy is given by the product:

$$\mathcal{H}_{\rm exc} = -\sum_{i<j} \left[S_x^i, S_y^i, S_z^i\right] \begin{bmatrix} J_{xx} & J_{xy} & J_{xz} \\ J_{yx} & J_{yy} & J_{yz} \\ J_{zx} & J_{zy} & J_{zz} \end{bmatrix} \begin{bmatrix} S_x^j \\ S_y^j \\ S_z^j \end{bmatrix}. \tag{6}$$

The basis of SD for a set of coupled spins is the integration of the stochastic Landau-Lifshitz equation for each localized magnetic moment $\vec{S}_i$:

$$\dot{\mathbf{S}}_i = -\gamma[\mathbf{S}_i \times \mathbf{H}_i] - \gamma\alpha[\mathbf{S}_i \times [\mathbf{S}_i \times \mathbf{H}_i]] \tag{7}$$

Here $\mathbf{H}_i = \vec{\xi}_i(t) - \partial\mathcal{H}/\partial\vec{\mu}_i$, with $\vec{\mu}_i$ the spin magnetic moment, is the local effective field which includes Zeeman, exchange, anisotropy and magnetostatic contributions, augmented by a stochastic term $\vec{\xi}_i(t)$ (which appears as an effective field). It is defined through the correlators:

$$\langle \xi_i(t) \rangle = 0, \quad \langle \xi_{i\eta}(t)\xi_{j\nu}(t') \rangle = \frac{2\alpha k_B T}{\gamma\mu_s}\delta(t-t')\delta_{ij}\delta_{\eta\nu}. \tag{8}$$

Here T is the temperature of the heat bath, γ is the gyromagnetic ratio, μ_s is the magnetic moment, α is the parameter describing the coupling strength to the heat bath, η and ν are Cartesian components. The basis of this equation is the separation of timescales, assuming that the bath (phonon or electron system) is much faster than the spin system. Consequently, the fluctuation-dissipation theorem can be applied to derive the equilibrium white noise properties of Eq. (8).

Although the Spin Dynamics approach can be used for the calculation of equilibrium properties such as $M(T)$, it is more computationally efficient to use the Monte-Carlo technique [28]. The temperature dependence of anisotropy is more complex. We note that this arises from magnetization fluctuations at elevated temperatures: the intrinsic anisotropy at the atomic level can be taken as temperature independent in the first instance. In order to calculate the anisotropy one must investigate the free energy surface at a non-zero temperature. This can be done using the constrained Monte-Carlo model of Asselin et.al. [29] which modifies the standard Metropolis approach by choosing moves of pairs of spins such that the overall magnetization direction is conserved. This approach allows exploration of the anisotropy free energy surface and the calculation of $K(T)$.

3.2. The atomistic spin Hamiltonian for $Nd_2Fe_{14}B$

Table 1: Summary table of model parameters and their units

Fe		
	$\mu_{\rm Fe}$	$2.2\ \mu_{\rm B}$
	$k_2^{\rm Fe}$	1.835×10^{-23} J/atom
Exchange $J_{ij}(r)$		
	J_0	-0.375×10^{-21} J
	$J_{\rm r}$	60.38×10^{-21} J
	r_0	1.25094 Å
	$r_{\rm cut}$	5.0 Å
Nd		
	$\mu_{\rm Nd}$	$3.2\ \mu_{\rm B}$
	$\kappa_2^{\rm Nd}$	$+1.889 \times 10^{-21}$ J/atom
	$\kappa_4^{\rm Nd}$	-1.007×10^{-21} J/atom
	$J_{\rm NdFe}$	6.291×10^{-22} J/link
	$r_{\rm cut}$	4.0 Å

Given the crystal structure of the $Nd_2Fe_{14}B$ crystal, we have formulated a Heisenberg spin Hamiltonian $\mathcal{H}$ which describes the energetics of the system in terms of energy contributions of the Nd and Fe sublattices:

$$\mathcal{H} = \mathcal{H}_{\rm Nd} + \mathcal{H}_{\rm Fe} \tag{9}$$

$$\mathcal{H}_{\rm Nd} = -\sum_{i<\delta} J_{\rm NdFe}\mathbf{S}_i \cdot \mathbf{S}_\delta - \sum_i E_i^{k,{\rm Nd}} - \mu_{\rm Nd}\sum_i \mathbf{H}_{\rm app} \cdot \mathbf{S}_i \tag{10}$$

$$\mathcal{H}_{\rm Fe} = -\sum_{\nu<\delta} J_{\rm Fe}(r)\mathbf{S}_\nu \cdot \mathbf{S}_\delta - \sum_{\nu<j} J_{\rm NdFe}\mathbf{S}_\nu \cdot \mathbf{S}_j - \sum_\nu E_\nu^{k,{\rm Fe}} - \mu_{\rm Fe}\sum_\nu \mathbf{H}_{\rm app} \cdot \mathbf{S}_\nu \tag{11}$$

where $\mathbf{S}$ are unit vectors describing the direction of the magnetic moments at each atomic site, i, j label Nd sites with moment $\mu_{\rm Nd}$, ν, δ label Fe sites with moment $\mu_{\rm Fe}$ and $\mathbf{H}_{\rm app}$ is the externally applied magnetic field vector. $J_{\rm NdFe}$ is the Fe-Nd nearest neighbor exchange energy, treated as

constant, and $J_{\mathrm{Fe}}(r)$ is the Fe-Fe exchange between Fe sites, treated as a function of interatomic separation r up to a cut-off distance r_{cut}, given by

$$J_{\mathrm{Fe}}(r) = J_0 + J_r \exp\left(-r/r_0\right) \tag{12}$$

where J_0 and J_r are fitting constants and r_0 is a characteristic distance. $E_i^{k,\mathrm{Nd}}$ and $E_\nu^{k,\mathrm{Fe}}$ describe the local magnetocrystalline anisotropy on the Nd and Fe sites respectively, and depend on second order, and for Nd, fourth order, anisotropy constants κ_2 and κ_4. Because of the lack of *ab-initio* data, formulation of the Hamiltonian and determination of the model parameters relies on fitting to experimental data: a complex process described elsewhere [30]. Full details of the final model parameters are detailed in Tab. 1. Calculations of magnetic properties and scaling laws using the above spin Hamiltonian have been carried out using the VAMPIRE software package [31]. The equilibrium temperature dependent properties of the system are calculated using the Monte Carlo metropolis method [28] integrated with the Hinzke-Nowak combinational algorithm [32].

The equilibrium properties of the system are obtained by performing 10,000 Monte Carlo steps at each temperature before calculating average magnetic properties over a further 20,000 steps. When calculating temperature dependent properties the final spin configuration from the previous temperature calculation is used to reduce the number of time steps required to reach thermal equilibrium at the new temperature.

4. Numerical coarse graining approach

The atomistic spin model has been used to investigate the finite size scaling of the magnetic properties for $Nd_2Fe_{14}B$. The approach used is to simulate a large cell with periodic boundary conditions to ensure a good approximation to bulk properties. Within the computational cell we average properties over a smaller cell in order to evaluate the cell-size and temperature dependent properties relevant for micromagnetic models. In addition to the $Nd_2Fe_{14}B$, For comparison we have also applied the model to a generic bcc system. The results are given in Fig. 3, which shows the scaling of the temperature dependence of the magnetization with cell size for $Nd_2Fe_{14}B$ and, for comparison a generic bcc system with nearest-neighbour Heisenberg exchange. The results for the Heisenberg exchange are consistent with the previous work of Kirschner et. al. [33]. Interestingly, there is a slightly smaller cell size scaling in the case of $Nd_2Fe_{14}B$. This is perhaps surprising given the large unit cell size of $Nd_2Fe_{14}B$, it is likely to be associated with the larger anisotropy of $Nd_2Fe_{14}B$.

5. Results

5.1. Atomistic model of DW pinning at interfaces

The microstructural features and grain interfaces have a strong bearing on the local anisotropy, and consequently

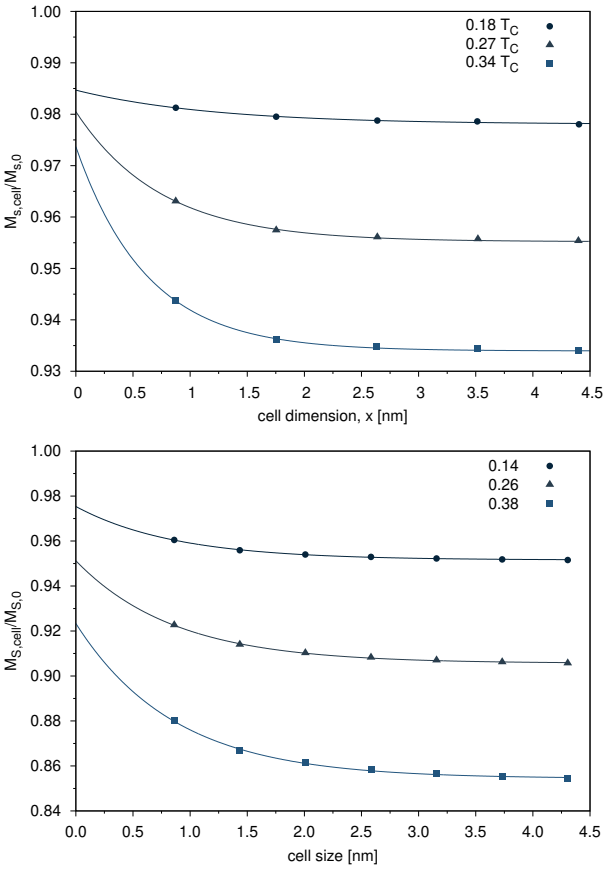

Figure 3: Scaling of the temperature dependence of the magnetization with cell size for $Nd_2Fe_{14}B$ (top panel) and a generic bcc system with nearest- neighbour Heisenberg exchange (lower panel).

on nucleation processes which may be a primary cause of the weakened coercivity seen in manufactured $Nd_2Fe_{14}B$-based sintered magnets [14]. Here we use the MD calculations outlined earlier to provide the equilibrium positions of atoms across the interface, which are used to calculate the local magnetic anisotropy arising from strain due to the lattice mismatch. This is done using the Néel pair anisotropy model, which allows us to calculate the local magnetoelastic strain for each atom in the system. As suggested be Néel [34], the leading contribution to the on-site anisotropy energy is given by

$$H_A = \sum_{i<j} L_{ij} (\boldsymbol{m}_i \cdot \boldsymbol{e}_{ij})^2 + \dots . \tag{13}$$

Here the vector $\boldsymbol{m}_i$ represents the spin on site i and the vector $\boldsymbol{e}_{ij}$ points from site i to each of its neighbours j. Both are normalised to unity. L_{ij} is the pair-anisotropy coupling and is dependent on the atomic separation between neighbours. Its magnitude is determined by fitting to the on-site anisotropy energy found by experiment. As a first approximation L_{ij} is set to decrease exponentially with r, the distance between neighbours, thereby taking into account the effects of local atomic order on the local MAE. Essentially the Néel model calculates anisotropy

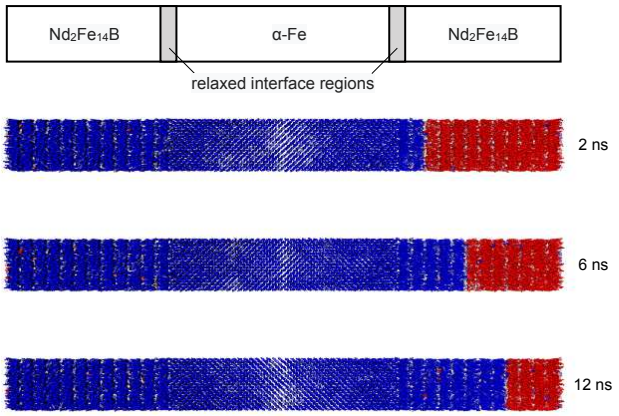

Figure 4: Snapshots showing the progress of a domain wall across an interface using the atomistic model with interface properties determined using a molecular dynamic model.

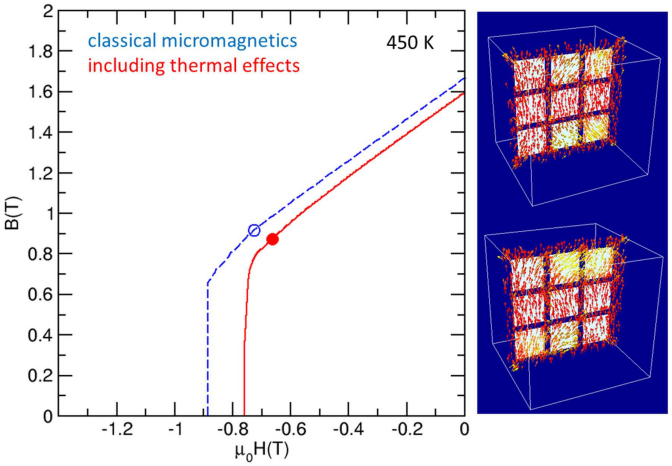

Figure 5: Influence of thermal fluctuations on remanence and coercivity in a nanocomposite permanent magnet. Left: (BH)-loop computed micromagnetically with and without thermal fluctuations. Right: magnetization in a slice through the magnet at different time for a fixed external field.

arising from symmetry breaking due to local strain.

We have used the atomistic Spin Dynamics model to investigate the propagation of a domain wall across a $Nd_2Fe_{14}B/\alpha$-Fe interface using anisotropy values determined from the atomic structures predicted by MD. The structure used is shown in Fig. 4 and consists of a nanowire with an α-Fe layer separating two $Nd_2Fe_{14}B$ sections. This is used so as to allow the application of antiferromagnetic periodic boundary conditions in order to force a domain wall into the system. Under the influence of an applied field the domain wall moves to the right. The snapshots in Fig. 4 show the motion of a domain wall crossing the interface. Interestingly, the motion is found to proceed by Barkhausen jumps discretised to the spacing of the planes of Nd sites.

5.2. Illustrative effects of cell-size scaling on micromagnetic properties

A key figure of merit for permanent magnets is the energy density product [35]. Its theoretical maximum, $\mu_0 M_s(T)^2/4$, depends on the magnetization squared. For magnets that are composed of multiple phases the volume averaged magnetization, $\bar{M}_s(T)$, has to be used. Long range wave length spin waves with a wave length comparable with the structural features reduce the remanent magnetization, $\mu_0 M_r$, with respect to the magnetization. The maximum achievable energy density product is

$$(BH)_{\max}(T) < \frac{\mu_0 M_r(T)^2}{4}, \qquad (14)$$

where $\bar{M}_s(T)$ depends on temperature and on the microstructure of the magnet. A prerequisite to achieve the energy density (14) is a coercive field larger than $\mu_0 M_r/2$. For an accurate computation of the energy density product by numerical micromagnetics at non-zero temperature the, the cell size corrected values for the magnetization have to be used. This is especially important when graded meshes are used in which the mesh size is adjusted to the microstructure.

A prominent example for multiphase permanent magnets are exchange spring magnets [1], in which a mixture of magnetically hard and soft phases is used to fine-tune the magnetic properties. The soft magnetic phase increases the remanent magnetization and the hard magnetic phase gives a sufficiently large coercive field provided that the exchange coupling between the different phases is strong enough. Micromagnetics helps to find optimal structures that maximise the energy density product. Bance et al. [6] showed that an optimal microstructure of a $Nd_2Fe_{14}B$ based exchange spring magnet consists of soft magnetic $Fe_{65}Co_{35}$ cubes embedded in a $Nd_2Fe_{14}B$ matrix. The thickness of the hard magnet phase which separates the soft magnetic cubes is around 4 nm. Fig. 5 compares the micromagnetically computed (BH)-loop for $T = 450$ K with and without thermal fluctuations. The dashed line gives the demagnetization curve obtained with classical micromagnetics. At each field point we integrate equation (7) in its continuum form whereby we drop the stochastic term in the effective field. The solid line gives the (BH)-loop computed with thermal fluctuations. In order to compute the reduction of the magnetization owing to long wave length spin waves, we used the magnetization configurations $M(H)$ as input for simulations including the stochastic fluctuation field. We scaled the magnetization that is used as input for the simulations according to the local mesh size of the finite element mesh and used results from section 4 based on the scaling procedure outlined by Kirschner *et al.* [33]. The new curve $M'(H,T) < M(H)$ includes the effect of thermal fluctuations on the magnetization. It is computed by averaging the magnetization over time for a fixed external field. The right hand side of Fig. 5 shows snapshots of the magnetization configurations at different times for $\mu_0 H_{\text{ext}} = -0.2$ T. The bright squares

in the slice through the magnet refer to the soft magnetic phase. Comparing the magnetization in the two images, we clearly see the fluctuations of the magnetization within the soft phase. The influence of thermal fluctuations on the coercive field [36] was computed by taking into account the escape time of the system over the finite energy barrier that separated the magnetic states before and after irreversible switching.

6. Summary and a missing link

We have developed a multiscale approach to the modelling of advanced permanent magnets. The basis of the model is a coupling and linking technique applied to the coarse graining of magnetic properties. Atomistic modelling is used to calculate the cell size scaling of the temperature dependent magnetic properties $M(T, L)$ and $K(T, L)$ which are subsequently used in a micromagnetic model to calculate hysteresis properties. Due to the large unit cell of $Nd_2Fe_{14}B$ the cell size scaling is stronger than for a nearest-neighbour Heisenberg model. The Atomistic Spin model has been linked to structure predictions from Molecular Dynamic modelling, which gives a detailed picture of interface structures and strain from which we calculate the local anisotropy in the interface. This is a powerful multiscale approach which allows realistic calculation of interface properties.

However, it should be noted that the parameters of the spin Hamiltonian of the atomistic model are determined by a detailed comparison with experiment. For 'parameter free' calculations, the spin Hamiltonian needs to be determined from *ab-initio* calculations as has been done for the specific case of FePt. [10] However, this process is difficult due to the origin of Rare-Earth magnetism in the 4f electrons, which is not well managed in DFT calculations. In principle it should be possible to solve this problem but the currently calculated parameters suffer from different approaches taken to the 4f electrons, however, it should be noted that the parameterisation of the atomistic spin model requires detailed (site-resolved) values of exchange and anisotropy. This is certainly a difficult problem and currently a missing link in the multiscale approach to permanent magnets which is currently being filled by fitting to experimental data. While this is a powerful approach and provides a strong basis for the understanding of structured permanent magnets, for example the detailed structure and properties of interfaces, more reliable and detailed DFT calculations are necessary for the next generation of material models.

7. Acknowledgements

This work is based on results obtained from the future pioneering program "Development of magnetic material technology for high-efficiency motors" commissioned by the New Energy and Industrial Technology Development Organization (NEDO).

[1] E. F. Kneller, R. Hawig, IEEE Trans. Magn. 27 (1991) 3588–3560.
[2] D. Givord, M. F. Rossignol, D. W. Taylor, J. Phys. IV France 2 (1992).
[3] T. G. Woodcock, Y. Zhang, G. Hrkac, G. Ciuta, N. M. Dempsey, T. Schrefl, O. Gutfleisch, D. Givord, Scr. Mater. 67 (2012) 536–541.
[4] J. Thielsch, D. Suess, L. Schultz, O. Gutfleisch, J. Appl. Phys. 114 (2013) 3–8.
[5] G. Hrkac, T. G. Woodcock, C. Freeman, A. Goncharov, J. Dean, T. Schrefl, O. Gutfleisch, Appl. Phys. Lett. 97 (2010) 98–101.
[6] S. Bance, H. Oezelt, T. Schrefl, M. Winklhofer, G. Hrkac, G. Zimanyi, O. Gutfleisch, R. F. L. Evans, R. W. Chantrell, T. Shoji, M. Yano, N. Sakuma, A. Kato, A. Manabe, Appl. Phys. Lett. 105 (2014) 192401.
[7] V. V. Dobrovitski, M. I. Katsnelson, B. N. Harmon, Phys. Rev. Lett. 84 (2000) 3458–3461.
[8] G. Grinstein, R. H. Koch, Phys. Rev. Lett. 90 (2003) 207201.
[9] R. E. Rottmayer, S. Batra, D. Buechel, W. A. Challener, J. Hohlfeld, Y. Kubota, L. Li, B. Lu, C. Mihalcea, K. Mountfield, K. Pelhos, C. Peng, T. Rausch, M. A. Seigler, D. Weller, X. M. Yang, IEEE Trans. Magn. 42 (2006) 2417–2421.
[10] N. Kazantseva, D. Hinzke, U. Nowak, R. W. Chantrell, U. Atxitia, O. Chubykalo-Fesenko, Phys. Rev. B Condens. Matter 77 (2008) 184428.
[11] O. N. O. N. Mryasov, U. Nowak, K. Y. Y. Guslienko, R. W. R. W. Chantrell, EPL 69 (2005) 805.
[12] I. Radu, K. Vahaplar, C. Stamm, T. Kachel, N. Pontius, H. A. Dürr, T. A. Ostler, J. Barker, R. F. L. Evans, R. W. Chantrell, A. Tsukamoto, A. Itoh, A. Kirilyuk, T. Rasing, A. V. Kimel, Nature 472 (2011) 205–208.
[13] T. A. Ostler, J. Barker, R. F. L. Evans, R. W. Chantrell, U. Atxitia, O. Chubykalo-Fesenko, S. El Moussaoui, L. Le Guyader, E. Mengotti, L. J. Heyderman, F. Nolting, A. Tsukamoto, A. Itoh, D. Afanasiev, B. A. Ivanov, A. M. Kalashnikova, K. Vahaplar, J. Mentink, A. Kirilyuk, T. Rasing, A. V. Kimel, Nat. Commun. 3 (2012) 666.
[14] G. Hrkac, T. G. Woodcock, C. Freeman, A. Goncharov, J. Dean, T. Schrefl, O. Gutfleisch, Appl. Phys. Lett. 97 (2010) 98–101.
[15] W. Mo, L. Zhang, Q. Liu, A. Shan, J. Wu, M. Komuro, Scr. Mater. 59 (2008) 179–182.
[16] J. D. G. Gale, Kristallogr. 220 (2005) 552–554.
[17] B. G. Dick, A. W. Overhauser, Phys. Rev. 112 (1958) 90–103.
[18] Y. Chen, S. Hirosawa, S. Iwata, Mater. Sci. Forum (2010).
[19] P. Morin, D. Schmitt, Vol. 5North-Holland, Amsterdam (1990).
[20] M. D. Kuz'min, J. M. Coey, Phys. Rev. B Condens. Matter 50 (1994) 12533–12539.
[21] C. Rudowicz, J. Phys. C: Solid State Phys. (1985).
[22] C. H. de Groot, K. de Kort, J. Appl. Phys. 85 (1999) 8312–8316.
[23] P. A. Algarabel, M. R. Ibarra, C. Marquina, A. del Moral, S. Zemirli, J. Magn. Magn. Mater. 84 (1990) 109–114.
[24] J. Barker, R. W. Chantrell, Phys. Rev. B Condens. Matter 92 (2015) 094402.
[25] O. N. Mryasov, Phase Transitions 78 (2005) 197–208.
[26] O. N. O. N. Mryasov, U. Nowak, K. Y. Y. Guslienko, R. W. R. W. Chantrell, EPL 69 (2005) 805.
[27] L. Udvardi, J. Jackson, U. Nowak, R. Chantrell, Phys. Rev. B: Condens. Matter Mater. Phys. (2011).
[28] N. Metropolis, A. W. Rosenbluth, M. N. Rosenbluth, A. H. Teller, E. Teller, J. Chem. Phys. 21 (1953) 1087–1092.
[29] P. Asselin, R. F. L. Evans, J. Barker, R. W. Chantrell, R. Yanes, O. Chubykalo-Fesenko, D. Hinzke, U. Nowak, Phys. Rev. B: Condens. Matter Mater. Phys. 82 (2010) 054415.
[30] R. F. L. Evans, R. Cuadrado, M. Probert, T. Shoji, M. Yano, A. Manabe, D. Givord, G. Hrkac, T. Schrefl, R. W. Chantrell (to be published).
[31] R. F. L. Evans, W. J. Fan, P. Chureemart, T. A. Ostler, M. O. A. Ellis, R. W. Chantrell, C. P, J. Phys. Condens. Matter 26 (2014) 103202.
[32] D. Hinzke, U. Nowak, Comput. Phys. Commun. 121 (1999) 334–337.

[33] M. Kirschner, T. Schrefl, F. Dorfbauer, G. Hrkac, D. Suess, J. Fidler, J. Appl. Phys. 97 (2005) 2004–2006.
[34] L. Neel, J. Phys. Radium 15 (1954) 92.
[35] J. Coey, Scr. Mater. 67 (2012) 524–529.
[36] J. Fischbacher, A. Kovacs, H. Oezelt, M. Gusenbauer, T. Schrefl, L. Exl, D. Givord, N. M. Dempsey, G. Zimanyi, M. Winklhofer, G. Hrkac, R. Chantrell, N. Sakuma, M. Yano, A. Kato, T. Shoji, A. Manabe, Appl. Phys. Lett. 111 (2017) 072404.